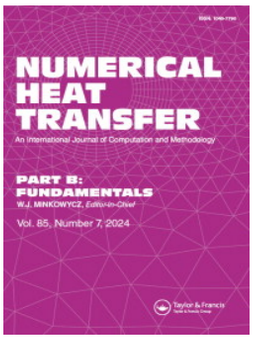


Taylor & Francis
Taylor & Francis Group

Numerical Heat Transfer, Part B: Fundamentals
An International Journal of Computation and Methodology

ISSN: (Print) (Online) Journal homepage: www.tandfonline.com/journals/unhb20

# Computational workflow to monitor the electroosmosis of nanofluidic flow in the vicinity of a bounding surface

E. G. Ghania, Sara I. Abdelsalam, A. M. Megahed, A. E. Hosni & A. Z. Zaher

**To cite this article:** E. G. Ghania, Sara I. Abdelsalam, A. M. Megahed, A. E. Hosni & A. Z. Zaher (14 Jun 2024): Computational workflow to monitor the electroosmosis of nanofluidic flow in the vicinity of a bounding surface, Numerical Heat Transfer, Part B: Fundamentals, DOI: 10.1080/10407790.2024.2364767

**To link to this article:** https://doi.org/10.1080/10407790.2024.2364767

NUMERICAL HEAT TRANSFER, PART B: FUNDAMENTALS
https://doi.org/10.1080/10407790.2024.2364767



# Computational workflow to monitor the electroosmosis of nanofluidic flow in the vicinity of a bounding surface

E. G. Ghania[a], Sara I. Abdelsalam[b], A. M. Megahed[c], A. E. Hosni[a], and A. Z. Zaher[a,d]

[a]Basic Science Department, Faculty of Engineering, Shoubra-Benha University, Banha, Egypt; [b]Basic Science, Faculty of Engineering, The British University in Egypt, Al-Shorouk City, Cairo, Egypt; [c]Basic Science Department, Faculty of Science, Benha University, Banha, Egypt; [d]Basic Science, Faculty of Engineering, Benha National University (BNU), El-Obour, Egypt

**ABSTRACT**

This investigation studies the flow of a boundary layer with electroosmotic forces on a nanofluid with gyrotactic microorganisms along the vertical Riga plate. This sort of fluid movement necessitates specific mathematical techniques and numerical simulations. In addition, the boundary-layer flow is induced by the mass and heat transfer, Joule heating, and viscous dissipation. A mathematical model is simulated by non-linear partial differential equations (PDEs). The combination of PDEs is turned into a set of non-linear ordinary differential equations using proper transformations. Some analysis tools are used to investigate the morphological characteristics of the problem while applying suitable boundary conditions. The influence of parameters on the derived solutions is numerically and visually explained through sets of figures. It is elucidated that the concentration of the microorganisms reduces due to an increase in Lewis number which leads to a decrease in the motile microorganism's density profile. It is seen that the temperature distribution is improved when the chemical reaction and Casson parameter increase. In addition, we find that the application of electro-osmotic forces applied to the surfaces helps to dewater and separate microorganisms from incompressible solid and liquid mixtures.

**ARTICLE HISTORY**
Received 26 February 2024
Revised 20 May 2024
Accepted 2 June 2024

**KEYWORDS**
Boundary layer; electroosmotic forces; Casson fluid model; numerical solution; electromagnetized plate

## 1. Introduction

A boundary layer is a liquid film that exists directly adjacent to a bounding surface and is impacted by viscosity. The gas or liquid boundary layer prefers to adhere to the surface. One of the well-known applications for the boundary layer is the dewatering effect. The dewatering effect is simply the deliberate removal of groundwater or surface water from an area. Dewatering is used to keep the ground dry so that concreting may take place. Linghui et al. [1] used the finite difference method to study the dewatering properties in a foundation with partial penetrating curtains. They deduced that the 3D flow improves dewatering efficiency significantly. The applications of the boundary layer are taken to another important level when non-Newtonian flows are involved. Nadeem and Rehman [2] used the Runge-Kutta Fehlberg to inspect the boundary layer of a Casson fluid with nanoparticles along a stretching cylinder. It was deduced that the distribution of temperature is enhanced by Reynolds number. Malik et al. [3] introduced analytical research to investigate the stream of the boundary layer with a non-Newtonian fluid using similarity solutions. It was found that the fluid temperature is maximum at the tube surface under

CONTACT Sara I. Abdelsalam sara.abdelsalam@bue.edu.eg Basic Science, Faculty of Engineering, The British University in Egypt, Al-Shorouk City, Cairo, Egypt.

consideration. Naseer et al. [4] shed light on the numerical resolutions of the boundary layer of a hyperbolic tangent fluid with heat transfer oriented axially of a vertical stretchable cylinder where it was seen that the flow slows down with enhanced values of the natural convection parameter. Khaled and Khan [10] conducted research about the inclusion of activation energy in a bioconvective flow model of a Casson fluid with nanoparticles and gyrotactic microorganisms where a thinning in the thermal boundary layer was noticed with an enhancement in the Prandtl number.

The incorporation of gyrotactic microorganisms into the nanoflow is critical for improving the thermal performance of several systems, including microfluidic devices, bacteria-powered micromixers, microbial fuel cells, and bio-microsystems. Asgari et al. [5] researched wastewater treatment plants (also known as 'WWTPs'). They concluded that the low-rated microbial growth is one of the important biological limitations in the process of sludge reduction along with the magnetic field that was further used to reduce the sludge volume index. The development of filamentous bacteria has been used in sludge management, and for the sake of decreasing the hydration of sludge, polyelectrolytes for the dewatering have sometimes been used as seen by Skinner et al. [6] and Marta and Feliks [7], respectively. The involvement of gyrotactic microorganisms and nanoparticles in bioconvection analysis was studied by Ahmad et al. [8] where it was seen that the motile micro-organisms' density is grown by growing the value of the parameter of motile microbes. A numerical investigation has been introduced by Basha and Sivaraj [9] studying the nanofluidic flow of blood for a non-Newtonian fluid with gyrotactic microorganisms. They concluded that the heat transfer rate is boosted by progressive values in the radiation parameter.

Nanofluid has recently achieved an outstanding status among scholars due to its efficient thermal behavior and significant conceivable applications. Hayat et al. [11] addressed a nanofluidic flow model for Casson fluid in a stretching cylinder through a boundary layer. It was demonstrated that the yield stress decreases with an augmentation in the Casson fluid parameter. Rafique et al. [12] used numerical techniques to investigate the flow boundary layer for a Casson model with nanoparticles with Dufour and Soret effects. It was discovered that increasing the Casson fluid parameter causes the flow to decelerate. Nadeem et al. [13] researched the inclined stagnation point for a Casson nanoflow with convective constraints where it was noticed that nanofluids can be utilized as an effective factor for controlling the rate of heat conduction at the interface. For more work involving nanofluids in potential applications, the reader is directed to refs. [14–25] and to the references in that matter.

The Riga plate is an electromagnetic plate on which conductors are alternately built. This configuration produces electromagnetic phenomena in the flowing fluid. Pantokratotas and Magyari [26] investigated the electro-magneto-hydrodynamics of a boundary-layer inflow over a Riga plate where it was detected that at a large distance from the border of the porous plate, the topmost velocity approaches the value of 1. Eldabe et al. [27] investigated the viscous dissipation effect and Joule heating on the boundary layer past a stretchable Riga plate. It was seen that the microrotation allocation increases with any rise in the parameter of mixed convection. Shafiq et al. [28] researched the material properties of Walter's B flow with nanoparticles and dual stratification over a Riga plate. It was seen that the momentum and velocity of the boundary layer region decreased for the stretched Riga region. The boundary-layer nanofluidic flow generated by a variable-thickness Riga plate was investigated by Hayat et al. [29] where the flux of nanoparticles was assumed zero at the surface. It was found that increasing the thermophoresis parameter boosts the solutal boundary layer thickness. Naseem et al. [30] conducted analytical research about the characteristics of a third-grade nanoflow produced by a Riga plate utilizing the Cattaneo-Christov theory where the mass flux of nanoparticles was assumed zero. It was concluded that for progressive values of the thermal relaxation parameter, there is a reduction in the temperature distribution ultimately. Vaidya et al. [31] presented an article about the mixed convection for electrically conducting nanofluid over a slender Riga plate where it was observed that the flow accelerates for increased values of the modified Hartmann number. Among the researchers who studied the

movement of electrically-conducting nanofluid in the presence of various external influences [32, 33].

Taking the aforementioned studies into consideration, our main objective in this work is to shed some light on the study of the effect of boundary-layer inflow of EOF on nanofluidic flow with gyrotactic microorganisms over the vertical Riga plate. The boundary layer is induced by heat and mass transfer, Joule heating, and viscous dissipation. A package from the Mathematica program that is called parametric ND solve (version 10) is employed to elucidate the physical quantities of the problem subjected to proper constraints. The influence of the pertinent parameters on the obtained solutions is discussed numerically and illustrated graphically.

## 2. Boundary layer Forchheimer flow mathematical representation with EOF

Consider the electro-magnetohydrodynamic (EMHD) and EOF of an incompressible non-Newtonian nanofluid past a linearly electro-magnetized plate. In addition, gyrotactic bacteria move about inside the fluid. Also, EOF is applied on the electro-magnetized plate, see Figure 1.

### 2.1. Casson fluid model

The viscosity model [2, 11, 12] can be written as:

$$\tau_{ij} = \begin{cases} 2\left((\mu_B)_{nf} + {}^{p_y}/_{\sqrt{2\pi}}\right)e_{ij}, & \pi \succ \pi_c \\ 2\left((\mu_B)_{nf} + {}^{p_y}/_{\sqrt{2\pi}}\right)e_{ij}, & \pi \prec \pi_c \end{cases}. \tag{1}$$

As a non-dimensional parameter, the following value is introduced with $\pi_c$

$$\beta = \frac{(\mu_B)_{nf}\sqrt{2\pi_c}}{p_y}, \tag{2}$$

where $p_y$ and $\mu_B$ are the yielding stress and the plastic viscosity. Also, $\pi = e_{ij}e_{ij}$ such that $e_{ij}$ is the $(i,j)$ component of the rate of deformation. In addition, $\alpha$ indicates the upper-limit apparent viscosity coefficient.

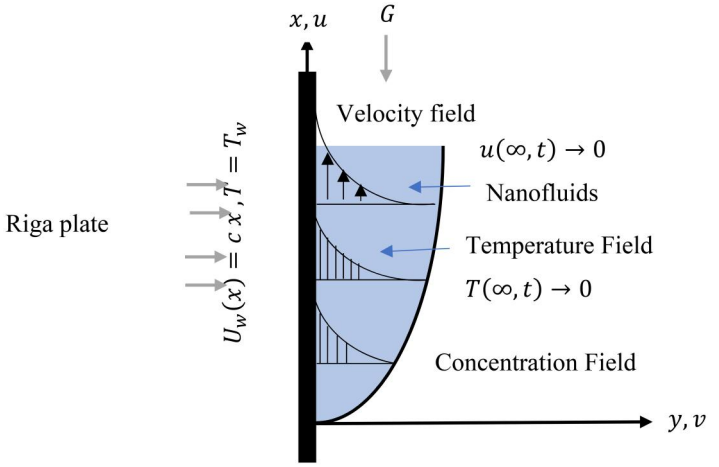


Figure 1. Physical interpretation of the boundary-layer model.

### 2.2. Equations governing the problem

The following are the governing equations that observe the boundary layer of the flowing fluid with EOF: momentum, continuity, microorganism, energy equation, and concentration equations [26–33]:

Equation of continuity:

$$\frac{\partial u}{\partial x}+\frac{\partial v}{\partial y}=0, \tag{3}$$

Equation of momentum:

$$\rho\left(u\frac{\partial u}{\partial x}+v\frac{\partial u}{\partial y}\right)=-\frac{\partial p}{\partial x}+\left(1+\frac{1}{\beta}\right)\frac{\partial^2 u}{\partial y^2}+G\beta_T(T-T_\infty)+G\beta_C(\varphi-\varphi_\infty)+\underbrace{\underbrace{\underbrace{\frac{nm_0\ j_0}{8\rho}}_{\text{electro magnetize plate}}+\underbrace{\rho_e E_x}_{\text{electroosmotic forces}}}_{\text{EOF}}}, \tag{4}$$

Energy equation:

$$(\rho C)_f\left(u\frac{\partial T}{\partial x}+v\frac{\partial T}{\partial y}\right)=K_T\left(\frac{\partial^2 T}{\partial x^2}+\frac{\partial^2 T}{\partial y^2}\right)+(\rho C)_p\left(D_B\nabla\varphi.\nabla T+\frac{D_T}{T_\infty}\nabla T.\nabla T\right), \tag{5}$$

Nanoparticle concentration:

$$u\frac{\partial \varphi}{\partial x}+v\frac{\partial \varphi}{\partial y}=D_B\left(\frac{\partial^2 \varphi}{\partial x^2}+\frac{\partial^2 \varphi}{\partial y^2}\right)+\frac{D_T}{T_\infty}\left(\frac{\partial^2 T}{\partial x^2}+\frac{\partial^2 T}{\partial y^2}\right)+K_0(\varphi-\varphi_\infty), \tag{6}$$

Gyrotactic microorganisms:

$$u\frac{\partial n}{\partial x}+v\frac{\partial n}{\partial y}=D_m\left(\frac{\partial^2 n}{\partial x^2}+\frac{\partial^2 n}{\partial y^2}+2\frac{\partial^2 n}{\partial yx}\right)-\frac{b\ w_c}{\varphi_w-\varphi_\infty}\left(\frac{\partial}{\partial y}\left(n\frac{\partial \varphi}{\partial y}\right)+\frac{\partial}{\partial x}\left(n\frac{\partial \varphi}{\partial x}\right)\right), \tag{7}$$

where $u$ and $v$ are the components of the velocity of fluid and the normal velocity in the $x$ and $y$ directions, consecutively. $(\rho c)_{f,p}$ is the fluid heat capacity and nanoparticle material, $k_T$ is the thermal conductivity, $D_B$ is the coefficient of Brownian diffusion, $D_T$ is the thermophoretic coefficient, $b$ is the constant of chemotaxis, $T_\infty$ is the local temperature, $n$ is the gyrotactic microorganisms, $D_m$ is the diffusivity of microorganisms and $W_c$ is the topmost swimming speed of the cells of microorganisms.

### 2.3. Analysis of EOF using boundary layer flow

One may derive from the Gaussian law the following [32]:

$$\nabla.E=\frac{\rho_e}{\varepsilon}, \tag{8}$$

Here, $\rho_e$ and $\varepsilon$ are the total ionic energy density and the permittivity of the dielectric, respectively. Because the electric field is considered a conservative one, the electric potential, $\overline{\Gamma}$, may be represented as [32]:

$$E = -\nabla\overline{\Gamma}, \tag{9}$$

The Poisson formula for the electrical potential propagation may be obtained by combining Eqs. (8) and (9) as follows [32]:

$$\nabla.\nabla\overline{\Gamma} = \nabla^2\overline{\Gamma} = -\frac{\rho_e}{\varepsilon}, \tag{10}$$

The total charge density that follows the Boltzmann dispersion is denoted by ref. [32].

$$\rho_e = -Z_\nu e(\overline{n}^- - \overline{n}^+), \tag{11}$$

such that the anions $\overline{n}^-$ and cations $\overline{n}^+$ are given by [32]:

$$\overline{n}^- = \overline{n}_0 e^{-\frac{eZ_\nu}{T_{av}K_B}\overline{\Gamma}}, \overline{n}^+ = \overline{n}_0 e^{+\frac{eZ_\nu}{T_{av}K_B}\overline{\Gamma}}, \tag{12}$$

where $\overline{n}_0$ is the concentration of bulk, $Z_\nu$ is the balance of charge, $K_B$ is the Boltzmann constant, $e$ the electronic charge and $T_{av}$ is the average temperature (the electrolytic solution's absolute temperature at the local level).

As reported by the Debye-Huckel linearization principle, $\frac{eZ_\nu}{T_{av}K_B} \ll 1$. And Eq. (16) reduces to [32, 34]:

$$\rho_e = \frac{\varepsilon}{\lambda_e^2}\overline{\Gamma},$$

Since the motion of fluid takes place in the boundary layer, then $\partial/\partial x \to 0$ in the left-hand side of Eq. (15) turns into [32, 34]

$$\frac{d^2\overline{\Gamma}}{dy^2} = \frac{1}{\lambda_e^2}\overline{\Gamma}. \tag{13}$$

where $\lambda_e = (eZ_\nu)^{-2}\frac{\varepsilon T_{av}K_B}{2n_0}$. By employing the following non-dimensional quantities [34]

$$\Gamma = \frac{\overline{\Gamma}}{\xi}, \eta = \sqrt{\frac{c}{\nu}}y, \tag{14}$$

Equation (19) reduces to [32, 34]

$$\frac{d^2\Gamma}{d\eta^2} = m_e^2\Gamma, \tag{15}$$

where $m_e\left(=\frac{\nu}{c\lambda_e^2}\right)$ is the electroosmotic parameter. The analytical expression of the above equation with boundary conditions $\Gamma = 1$ at $\eta = 0$ and $\Gamma \to \infty$ at $\eta \to \infty$ is found as [32, 34]:

$$\Gamma = \exp^{-m_e\eta}. \tag{16}$$

## 3. Non-dimensional transformations of similarity

Introducing the nondimensional similarity transformations

$$\psi = \sqrt{c\nu_f}xf(\eta), \theta = \frac{T - T_\infty}{T_w - T_\infty}, \Phi = \frac{\varphi - \varphi_\infty}{\varphi_w - \varphi_\infty}, \chi = \frac{n - n_\infty}{n_w - n_\infty}, \eta = \sqrt{\frac{c}{\nu}}y, \tag{17}$$

where $\psi$ is the stream function and is given as

$$u = \frac{\partial\psi}{\partial y} = cxf'(\eta), \quad v = -\frac{\partial\psi}{\partial x} = -\sqrt{c\nu_f}f(\eta). \tag{18}$$

By making use of Eqs. (17) and (18) in Eqs. (8–12), we deduce the next set of similarity equations:

$$\left(1+\frac{1}{\beta}\right)f''\prime(\eta)+\quad f(\eta)f''(\eta)-f'(\eta)^2+\lambda(\theta(\eta)-N\phi(\eta)-L_C\chi(\eta))+ \underbrace{Qe^{-\alpha y}}_{\text{electromagnetized}}+\underbrace{U_{hS}\ m_e^2 e^{-m_e\eta}}_{\text{electroosmoticforces}}=0, \tag{19}$$

EOF

$$\theta''(\eta)+\quad P_r(f(\eta)\theta'(\eta)+N_b\theta'(\eta)\Phi'(\eta))+N_t\theta'(\eta)^2, \\ =0, \tag{20}$$

$$\Phi''(\eta)+\frac{N_t}{N_b}\theta''(\eta)+L_e f(\eta)\Phi'(\eta)+L_e\gamma\ \Phi(\eta)=0, \tag{21}$$

$$\chi''(\eta)+L_b\chi'(\eta)f(\eta)-P_e\Big(\chi(\eta)\Phi'(\eta)+\big(\Omega+\chi(\eta)\big)\Phi''(\eta)\Big)=0. \tag{22}$$

Under conditions,

$$f(0)=0, f'(0)=1, \theta(0)=1, \Phi(0)=1, \chi(0)=1, \\ f'(\eta)\to 0, \theta(\eta)\to 0, \Phi(\eta)\to 0, \chi(\eta)\to 0, \text{ at } \eta\to\infty \tag{23}$$

where $\beta$, $\lambda$, $N$, $L_C$, Q, $U_{HS}$, $me$, $N_b$, $N_t, P_r$, $L_e$, $\gamma$, $L_b$, $\Omega$, and $P_e$, respectively, stand for the Casson number, the mixed convection parameter, the buoyancy ratio parameter, the bioconvection Rayleigh number, the modified Hartman number, Helmholtz-Smoluchowski dimensionless velocity, the electroosmotic parameter, Brownian motion parameter, the thermophoresis parameter, Prandtl number, Lewis number, the chemical reactions, the bioconvection Schmidt number, the microorganism concentration difference parameter and the bioconvection Péclet number.

## 4. Theoretical findings and physical characteristics

As previously stated, a numerical solution to the nonlinear PDEs of EOF impact on the boundary-layer Casson nanoflow with gyrotactic microorganisms is constructed in the proposed study using the parametric NDSolve package in MATHEMATICA software. There are many significant interpretations for the dimensionless parameters such as Helmholtz-Smoluchowski dimensionless velocity $\boldsymbol{U_{HS}}$, electroosmotic parameter *me*, modified Hartmann number Q, Brownian motion parameter $\mathbf{N_t}$, thermophoresis parameter $\mathbf{N_b}$, and Prandtl number $\mathbf{P_r}$ which are discussed in the next subsections.

### 4.1. Results validity

The value of skin friction for Newtonian fluid is compared to the values reported by Magyari and Keller [35] and coincides with our results. Additionally, as shown in Table 1, a comparison of the outcomes corresponding to the values of the Nusselt number for a Newtonian fluid with the results of Magyari and Keller's [35] previously published work can be used to confirm the precision of the numerical approach used.

**Table 1.** Prandtl number values for Newtonian fluid at various of the Nusselt number values.

| Pr | Magyari and Keller's [33] | Present study with $U_{HS}=0$, $N_b=0$, $N_t=0$, $L_c=0$, Q = 0, $\beta=0$ |
|---|---|---|
| 1 | 0.9548 | 0.9548 |
| 3 | 1.8691 | 1.8691 |
| 5 | 2.5001 | 2.5001 |
| 10 | 3.6604 | 3.6604 |

### 4.2. Velocity profiles

The influence of Casson's number $\beta$, modified Hartman number Q, Helmholtz-Smoluchowski dimensionless velocity $U_{HS}$, Electroosmotic parameter *me*, mixed convection parameter $\lambda$ are seen and illustrated in Figure 2. It can be noticed in Figure 2(a) that the Casson number decreases the velocity profiles while the modified Hartmann number enhances the velocity of boundary-layer flow as seen in Figure 2(a). Figure 2(c, d) discusses the effect of Helmholtz-Smoluchowski dimensionless velocity $U_{HS}$ and electroosmotic parameter *me* on the velocity of boundary-layer flow. It can be demonstrated that the behavior of the velocity profile increases when the Helmholtz-Smoluchowski dimensionless velocity $U_{HS}$ and electroosmotic parameter *me* increase. This is due to the opposing ions' charges being drawn to the surfaces, and the ions from the surface undergoing the opposite process. Following this definition, the electric double layer (EDL) area shows up, and the fluid accelerates when the surface gets electrically charged. This is because of the introduction of an external electric field parallel to the solid surface causing counter-ions and co-ions to migrate toward the cathode and anode, drawing and accelerating analogous fluids. This helps to dewater and gyrotactic involved of liquid and solid incompressible blends. Figure 2(e) shows the effect of the parameter of $\lambda$ on the behavior of velocity. It is elucidated that as $\lambda$ is increased the boundary layer velocity increases.

### 4.3. Heat transfer profiles

Figure 3 exhibits the effect of the Helmholtz-Smoluchowski dimensionless velocity $U_{HS}$, electroosmotic parameter *me*, modified Hartman number Q, Brownian motion parameter $N_t$, thermophoresis parameter $N_b$ and Prandtl number $P_r$ on heat transfer. Figure 3(a) portrays the effect of the Helmholtz-Smoluchowski dimensionless velocity $U_{HS}$ and Electroosmotic parameter *me* on the temperature distribution $\theta(\eta)$. The temperature of the fluid increases as the electroosmotic parameter *me* increases for positive values of $U_{HS}$. In addition, the heat transfer is greater for negative values of $U_{HS}$ then for positive values of $U_{HS}$. Figure 3(b) discusses the effect of modified Hartmann number Q on the heat transfer where it is found that Q enhances the fluid temperature. Figure 3(c) discusses the influence of Prandtl number $P_r$ (the ratio between the momentum diffusion coefficient to the thermal diffusion coefficient) on the heat transfer. The latter dimensionless quantity is more applicable in studying the concept of boundary layers. It is noticed that the thermal conductivity of the liquid is reduced with an increase in the value of $P_r$, and the heat transfer slows down, which lowers the flow temperature, so a reduction in temperature is noticed. Figure 3(d) discusses the influence of $N_t$ on $\theta(\eta)$. Increasing the thermal transfer coefficient implies to an enhancement in the temperature of the liquid because in the process of thermal separation, the tiny particles travel from the high to the low-temperature area. Figure 3(e) depicts the effect of the Brownian diffusion coefficient ($N_b$) on $\theta(\eta)$. Brownian motion is defined as the haphazard motion of suspended particles in a liquid. It is natural to find that increasing the Brownian diffusion coefficient, improves the temperature transfer of the liquid and this occurs because of random collisions between suspended particles in the liquid. Figure 3(f, g) discusses the effect of a chemical reaction and Casson parameter on the distribution of temperature. It is seen that the temperature distribution $\theta(\eta)$ is improved when the chemical reaction and Casson parameter increase.

### 4.4. Concentration distribution (mass fraction field)

Figure 4 exhibits the influence of $U_{HS}$, *me*, Q, $N_t$, and $N_b$ on the mass fraction field. Figure 4(a) demonstrates the impact of $U_{HS}$ and *me* on the mass fraction field $\phi(\eta)$. The mass fraction field increases as the electroosmotic parameter *me* increases for positive values of $U_{HS}$, while the opposite effect occurs for negative values $U_{HS}$. In addition, the mass fraction field is higher for

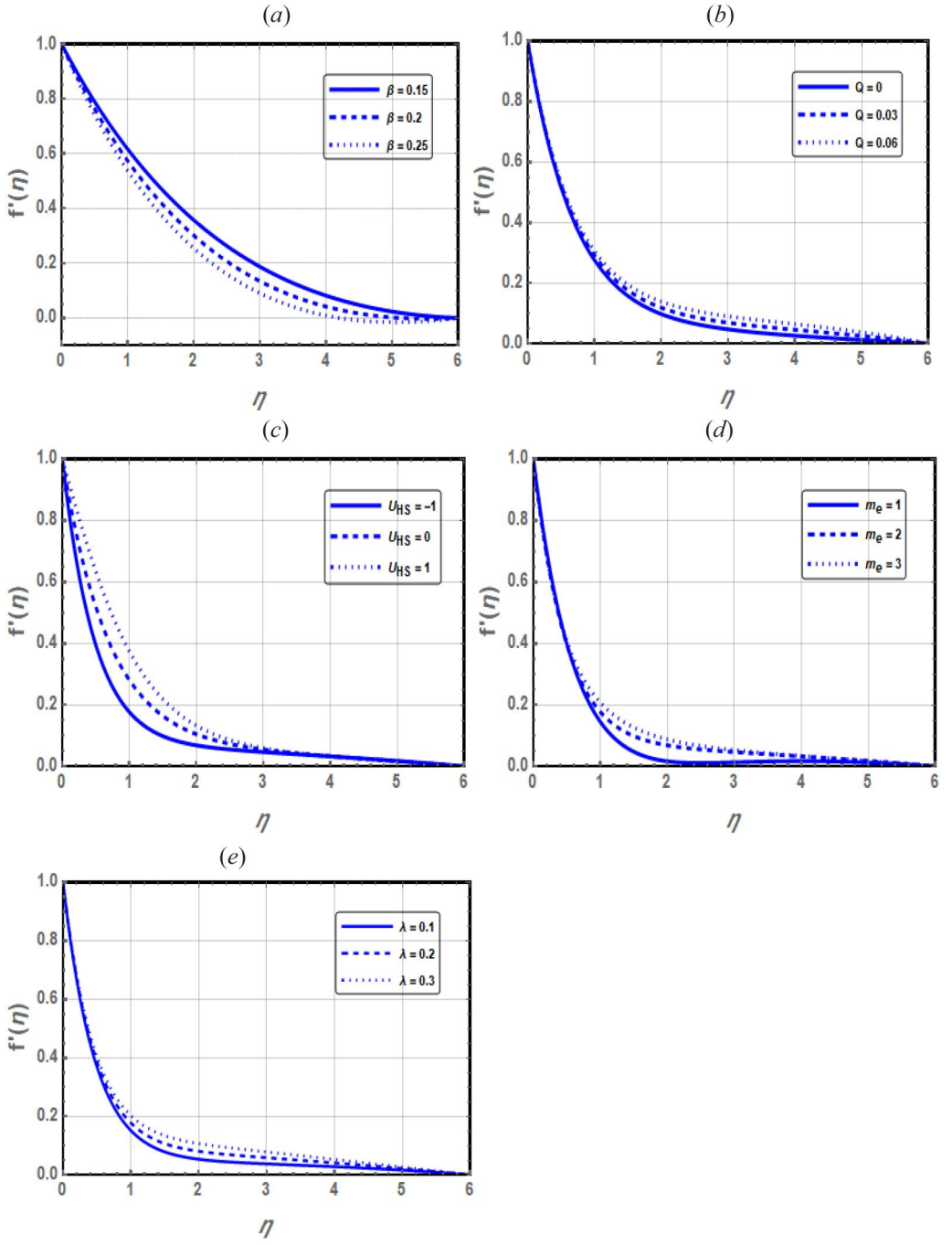


**Figure 2.** Velocity profiles for different parameters panel (a) $\beta$, (b) Q, (c) $U_{HS}$, (d) $m_e$, (e) $\lambda$.

negative values of $U_{HS}$ than for positive values of $U_{HS}$. Figure 4(b) discusses the impact of Q on $\phi(\eta)$. It is found that Q reduces $\phi(\eta)$. Figure 4(c) describes the effect of $N_t$ on $\phi(\eta)$. It was observed that nanoparticles get squashed with increasing $N_t$ values because the density of the concentration of the boundary layer increases, which causes an increase in $\phi(\eta)$. Figure 4(d) shows the effect of thermophoresis parameter $N_b$ on $\phi(\eta)$. It was found that the higher the values of the thermophoresis parameter $N_b$, the greater the random movement between the

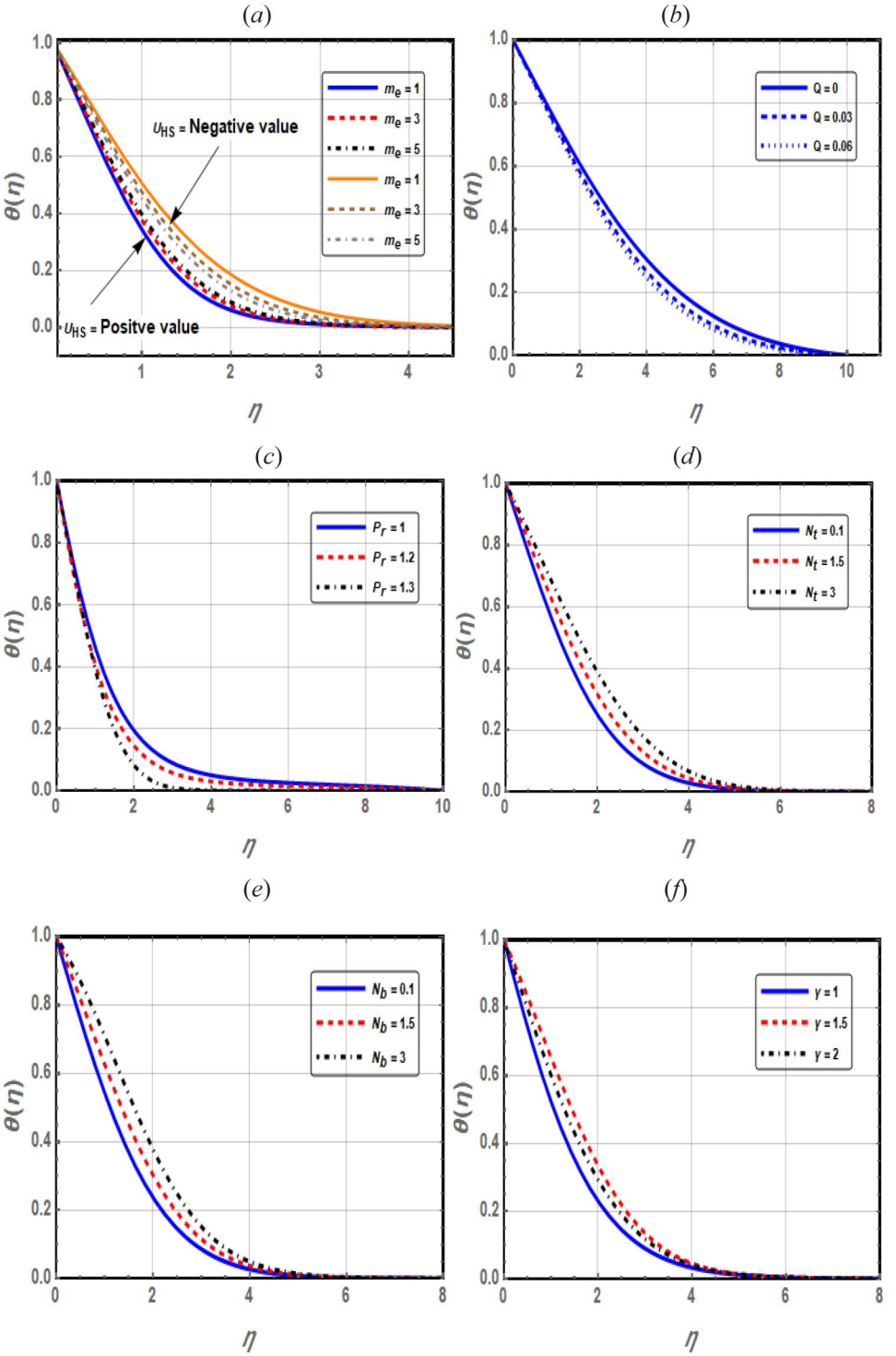


**Figure 3.** Heat transfer profiles for different parameters panel (a) $U_{HS}$ and $m_e$, (b) Q, (c) $P_r$, (d) $N_t$, (e) $N_b$, (f) $\gamma$, (g) $\beta$.

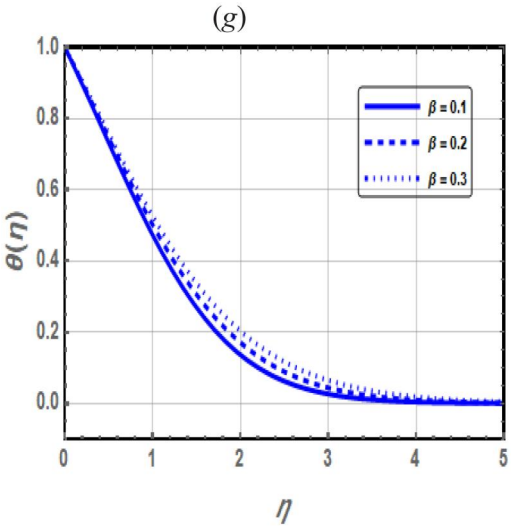


**Figure 3.** Continued.

nanoparticles that are present in the liquid. This implies a reduction in the concentration of fluid. Figure 4(e) demonstrates the effect of the Lewis number $L_e$ on the mass fracture field. It is known as the ratio between the thermal diffusion and mass diffusion The concentration profile is observed to drop owing to the Lewis number's dependency on the Brownian diffusion coefficient, which indicates that an increase in the Brownian diffusion coefficient causes a decrease in the concentration behavior. Figure 4(d) discusses the effect of chemical reactions on $\phi$ $(\eta)$ where it is seen that $\phi$ $(\eta)$ is improved when the chemical reaction increases.

### 4.5. Density profile of motile microorganisms

Figure 5 presents the impact of different parameters; Helmholtz-Smoluchowski dimensionless velocity $U_{HS}$, modified Hartmann number Q, bioconvection Péclet number $P_e$, parameter of microorganism concentration difference $\Omega$, Lewis number $L_e$ and bioconvection Schmidt number $L_b$ on the motile microorganism's density profile. Figure 5(a) depicts the effect of the Helmholtz-Smoluchowski dimensionless velocity $U_{HS}$ on the motile microorganisms' profile density. It is seen that the Helmholtz-Smoluchowski dimensionless velocity $U_{HS}$ reduces the motile microorganisms' density profile. This means that the application of the electroosmotic forces leads to the reduction of microorganisms in incompressible solid and liquid mixtures. Figure 5(b) demonstrates the impact of Q on the motile microorganism's density profile. It is demonstrated that the motile microorganism's profile density reduces for an increase in Q. Also, it is demonstrated that $P_e$ boosts the microorganism's distribution as shown in Figure 5(c). Figure 5(d) discusses $\Omega$ on the motile microorganism's profile density. These microorganisms spread through the material from a high-concentrated to a low-concentrated area. Through this, it was found that the spread of microorganisms is restricted, which makes them decrease in the case of an increase in $\Omega$. Hence, the motile microorganism's distribution decreases. Figure 5(e) depicts the impact of $L_e$ on the motile microorganism's distribution. As mentioned before, $L_e$ is known as the ratio between the thermal diffusion and diffusion of the motile microorganisms. It is elucidated that the concentration of the microorganisms reduces due to an increase in $L_e$ which leads to a decrease in the motile microorganism's density profile. Figure 5(f) delineates that the $L_b$ reduces the motile microorganism's density profile. In addition, in Figure 5(g), it is remarked that the Casson parameter enhances the motile microorganism's density profile.

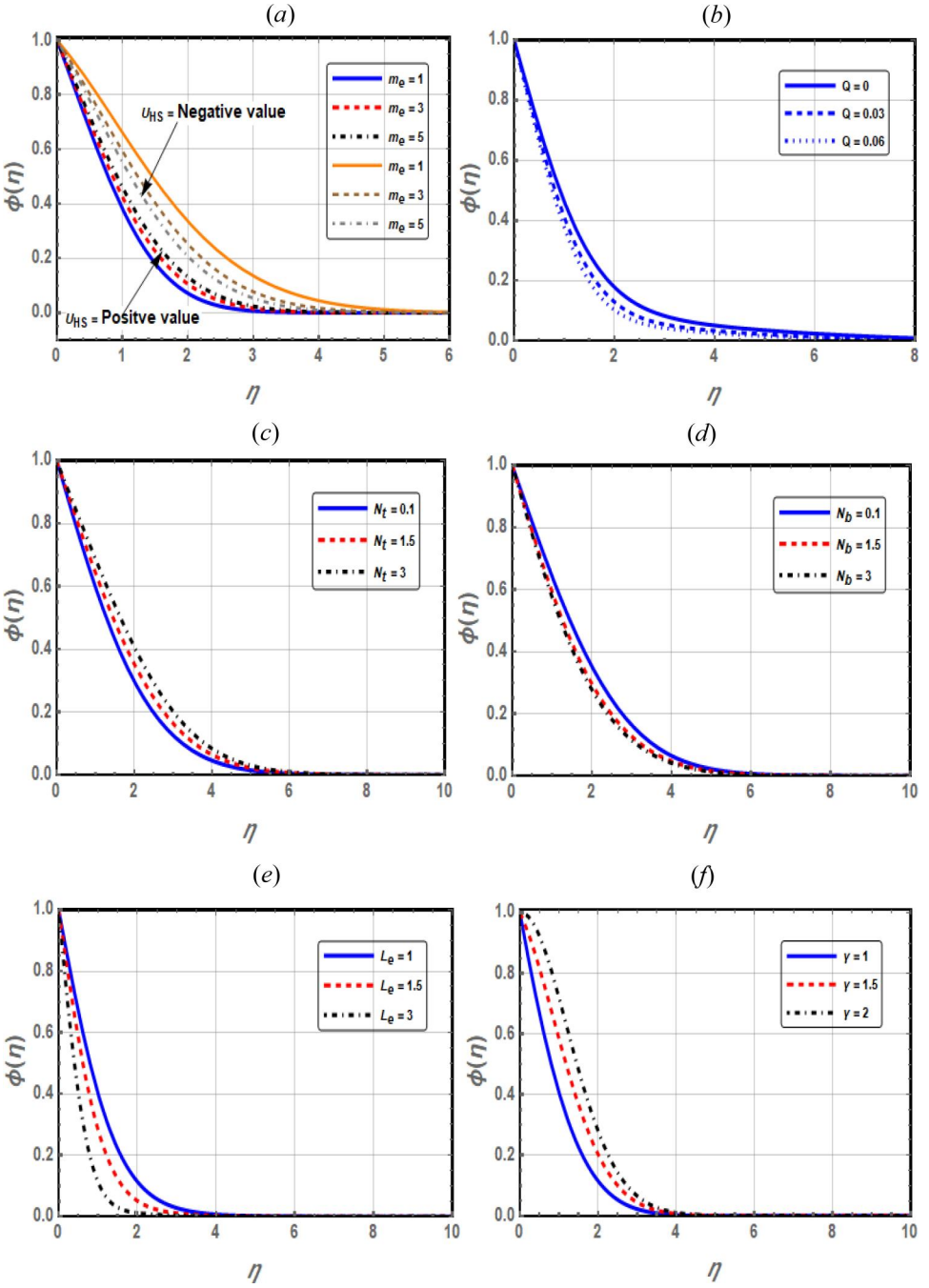


**Figure 4.** Mass fraction field profiles for different parameters panel (a) $U_{HS}$ and $m_e$, (b) Q, (c) $N_t$, (d) $N_b$, (e) $L_c$, (f) $\gamma$.

## 5. Outcomes and conclusions remarks

Heat and mass transfer of nanofluids by electroosmotic forces through boundary layer flow are discussed. The non-Newtonian fluid is simulated by Casson fluid in addition this non-Newtonian fluid contains a gyrotactic microorganism. A parametric ND Solve method (PNDS) is implemented to solve the package of nonlinear PDEs. The findings have been explained to give useful

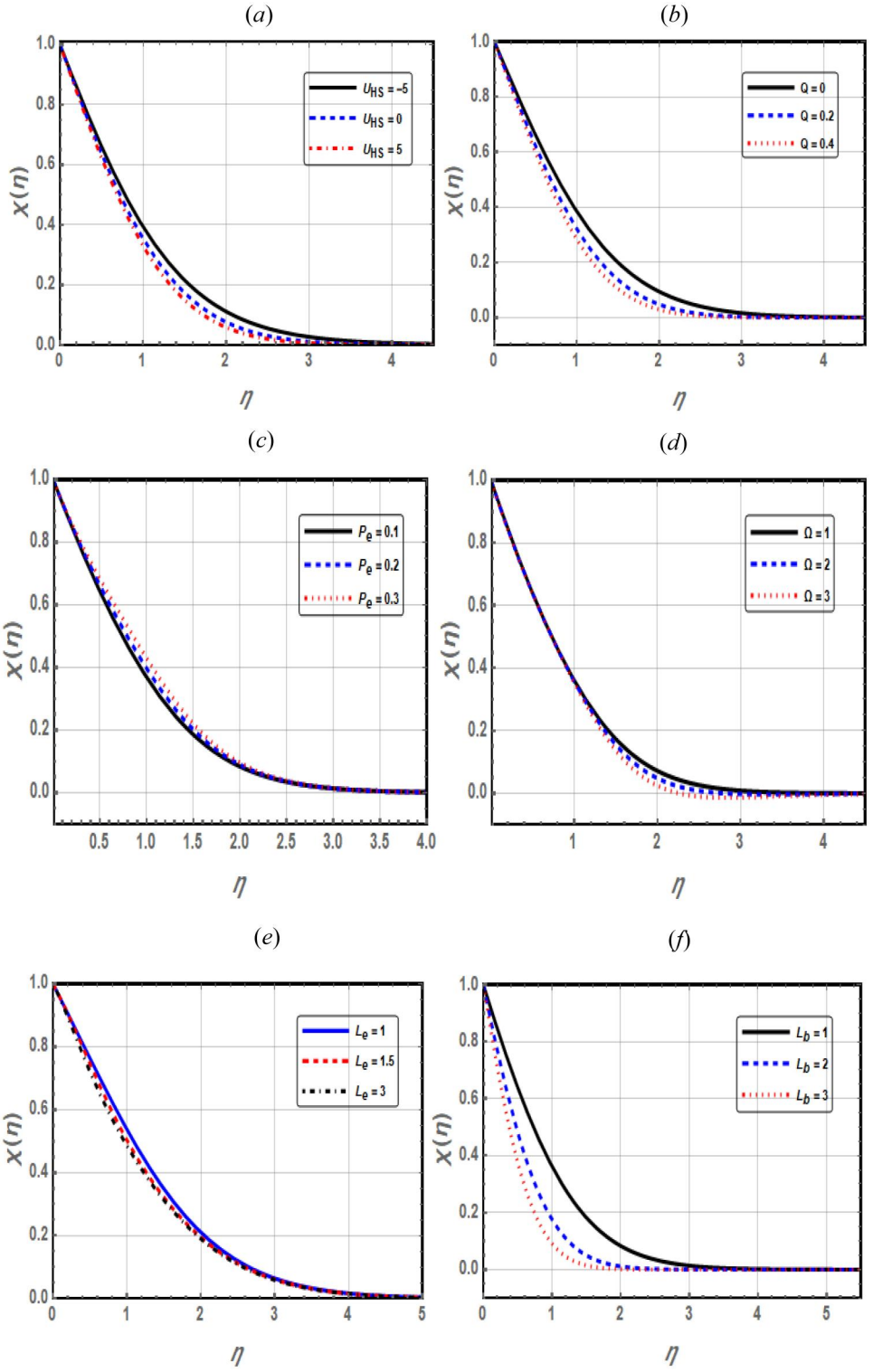


**Figure 5.** The motile micro-organisms density profile for different parameters panel (a) $U_{HS}$, (b) Q, (c) $P_e$, (d) Ω, (e) $L_e$, (f) $L_b$, (g) $\beta$.

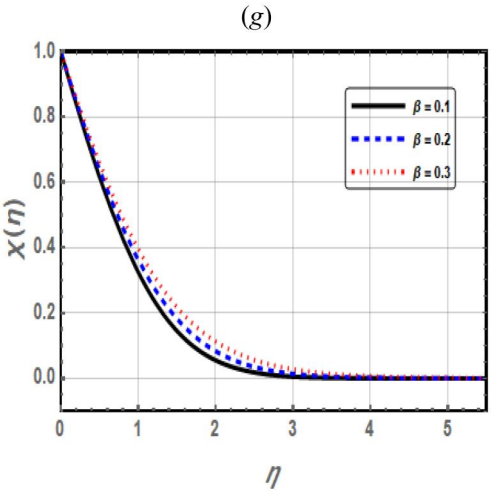


**Figure 5.** Continued.

information for researchers in biomedical engineering and other technical domains. It is sought that the proposed results will benefit the investigations involving the electric forces inflows of non-Newtonian models with microscopic microorganisms. The following key points emerge from the analysis of the graphs and table:

- The parameters of Brownian diffusion and thermal travel are shown as a result of the insertion of nanoparticles in the liquid.
- The electroosmotic parameter and the Helmholtz-Smoluchowski dimensionless velocity increase the boundary layer velocity which helps dewatering incompressible solid and liquid mixtures.
- The mass fraction field of nanofluids is greater for negative values of the Helmholtz-Smoluchowski dimensionless velocity $U_{HS}$ then for positive values of the Helmholtz-Smoluchowski dimensionless velocity $U_{HS}$.
- The modified Hartman number boosts the temperature of the nanofluids.
- The concentration of nanofluids is reduced due to the reliance on the Lewis number on the Brownian coefficient. This means that the increase in the Brownian coefficient leads to a reduction in the concentration profile.

## Disclosure statement

On behalf of all authors, the corresponding author states that there is no conflict of interest.

## Funding

Open access funding provided by The Science, Technology & Innovation Funding Authority (STDF) in cooperation with The Egyptian Knowledge Bank (EKB).

## ORCID

Sara I. Abdelsalam http://orcid.org/0000-0002-6434-8319

## Data availability statement

All data generated or analyzed during this study are included in this published article.

## References


[1] L. Liu, M. Lei, C. Cao, and C. Shi, "Dewatering characteristics and inflow prediction of deep foundation pits with partial penetrating curtains in sand and gravel strata," *Water*, vol. 11, no. 10, pp. 2182, 2019. DOI: 10.3390/w11102182.

[2] M. Y. Malik, M. Naseer, S. Nadeem, and A. Rehman, "The boundary layer flow of Casson nanofluid over a vertical exponentially stretching cylinder," *Appl. Nanosci.*, vol. 4, no. 7, pp. 869–873, 2014. DOI: 10.1007/s13204-013-0267-0.

[3] M. Y. Malik, A. Hussain, and S. Nadeem, "Boundary layer flow of an Eyring–Powell model fluid due to a stretching cylinder with variable viscosity," *Sci. Iran.*, vol. 20, no. 2, pp. 313–321, 2013. DOI: 10.1016/j.scient.2013.02.028.

[4] M. Naseer, M. Y. Malik, S. Nadeem, and A. Rehman, "The boundary layer flow of hyperbolic tangent fluid over a vertical exponentially stretching cylinder," *Alex. Eng. J.*, vol. 53, no. 3, pp. 747–750, 2014. DOI: 10.1016/j.aej.2014.05.001.

[5] G. Asgari, R. Khoshniyat, and H. Shabrandi, "Effect of magnetic fields on the sludge properties in the aeration basin of the activated sludge treatment process," *Int. J. Waste Resour.*, vol. 11, no. 5, pp. 1–8, 2021. DOI: 10.35248/2252-5211.21.11.412.

[6] S. J. Skinner, *et al.*, "Quantification of wastewater sludge dewatering," *Water Res*, vol. 82, pp. 2–13, 2015. DOI: 10.1016/j.watres.2015.04.045.

[7] M. Wójcik and F. Stachowicz, "Influence of physical, chemical and dual sewage sludge conditioning methods on the dewatering efficiency," *Power Technol.*, vol. 344, pp. 96–102, 2019. DOI: 10.1016/j.powtec.2018.12.001.

[8] S. Ahmad, M. Ashraf, and K. Ali, "Bioconvection due to gyrotactic microbes in a nanofluid flow through a porous medium," *Heliyon*, vol. 6, no. 12, pp. e05832, 2020. DOI: 10.1016/j.heliyon.2020.e05832.

[9] H. Thameem and R. Sivaraj, "Numerical simulation of blood nanofluid flow over three different geometries by means of gyrotactic microorganisms: applications to the flow in a circulatory system," *J. Mech. Eng. Sci.*, vol. 235, no. 2, pp. 441–460, 2021. DOI: 10.1177/0954406220947454.

[10] K. Al-Khaled and S. U. Khan, "Thermal aspects of Casson nanoliquid with gyrotactic microorganisms, temperature-dependent viscosity, and variable thermal conductivity: bio-technology and thermal applications," *Inventions*, vol. 5, no. 3, pp. 39, 2020. DOI: 10.3390/inventions5030039.

[11] T. Hayat, S. Asad, and A. Alsaedi, "Flow of Casson fluid with nanoparticles," *Appl. Math. Mech.-Engl. Ed.*, vol. 37, no. 4, pp. 459–470, DOI: 10.1007/s10483-016-2047-9.

[12] K. Rafique, *et al.*, "Numerical solution of Casson nanofluid flow over a non-linear inclined surface with Soret and Dufour effects by Keller-box method," *Front. Phys.*, vol. 7, pp. 1–13, 2019. DOI: 10.3389/fphy.2019.00139.

[13] S. Nadeem, R. Mehmood, and N. S. Akbar, "Optimized analytical solution for oblique flow of a Casson-nano fluid with convective boundary conditions," *Int. J. Thermal Sci.*, vol. 78, pp. 90–100, 2014. DOI: 10.1016/j.ijthermalsci.2013.12.001.

[14] M. M. Bhatti and S. I. Abdelsalam, "Bio-inspired peristaltic propulsion of hybrid nanofluid flow with Tantalum (Ta) and Gold (Au) nanoparticles under magnetic effects," *Waves Random Complex Media*, vol. 34, pp. 1–26, 2021. DOI: 10.1080/17455030.2021.1998728.

[15] M. M. Bhatti, M. Marin, A. Zeeshan, and S. I. Abdelsalam, "Editorial: recent trends in computational fluid dynamics," *Front. Phys.*, vol. 8, pp. 593111 [1–4], 2020. DOI: 10.3389/fphy.2020.593111.

[16] R. M. Abumandour, I. M. Edesoky, M. H. Kamel, M. M. Ahmed, and S. I. Abdelsalam, "Peristaltic thrusting of a thermal-viscosity nanofluid through a resilient vertical pipe," *Z. Naturforsch. A*, vol. 75, no. 8, pp. 727–738, 2020. DOI: 10.1515/zna-2020-0054.

[17] A. Dawar and N. Acharya, "Unsteady mixed convective radiative nanofluid flow in the stagnation point region of a revolving sphere considering the influence of nanoparticles diameter and nanolayer," *J. Indian Chem. Soc.*, vol. 99, no. 10, pp. 100716, 2022. DOI: 10.1016/j.jics.2022.100716.

[18] N. Acharya, "Spectral quasi linearization simulation on the radiative nanofluid spraying over a permeable inclined spinning disk considering the existence of heat source/sink," *Appl. Math. Comput.*, vol. 411, no. 126547, pp. 126547, 2021. DOI: 10.1016/j.amc.2021.126547.

[19] N. Acharya, R. Bag, and P. K. Kundu, "Unsteady bioconvective squeezing flow with higher-order chemical reaction and second-order slip effects," *Heat Trans.*, vol. 50, no. 6, pp. 5538–5562, 2021. DOI: 10.1002/htj.22137.

[20] N. Acharya, S. Maity, and P. K. Kundu, "Differential transformed approach of unsteady chemically reactive nanofluid flow over a bidirectional stretched surface in presence of magnetic field," *Heat Trans.*, vol. 49, no. 6, pp. 3917–3942, 2020. DOI: 10.1002/htj.218153942.

[21] A. Shafiq and T. N. Sindhu, "Statistical study of hydromagnetic boundary layer flow of Williamson fluid regarding a radiative surface," *Results Phys.*, vol. 7, pp. 3059–3067, 2017. DOI: 10.1016/j.rinp.2017.07.077.

[22] T. Hayat, A. Shafiq, and A. Alsaedi, "Effect of Joule heating and thermal radiation in flow of third grade fluid over radiative surface," *PLoS ONE*, vol. 9, no. 1, pp. e83153, 2014. DOI: 10.1371/journal.pone.0083153.
[23] A. Shafiq, S. A. Lone, T. N. Sindhu, Q. M. Al-Mdallal, and G. Rasool, "Statistical modeling for bioconvective tangent hyperbolic nanofluid towards stretching surface with zero mass flux condition," *Sci. Rep.*, vol. 11, no. 1, pp. 13869, 2021. · DOI: 10.1038/s41598-021-93329-y.
[24] A. Shafiq, A. B. Çolak, and N. Sindhu, "Designing artificial neural network of nanoparticle diameter and solid–fluid interfacial layer on single-walled carbon nanotubes/ethylene glycol nanofluid flow on thin slendering needles," *Numer. Methods Fluids*, vol. 93, no. 12, pp. 3384–3404, 2021. DOI: 10.1002/fld.5038.
[25] A. Shafiq, A. B. Çolak, S. A. Lone, T. N. Sindhu, and T. Muhammad, "Reliability modeling and analysis of mixture of exponential distributions using artificial neural network," *Math. Methods Appl. Sci.*, vol. 47, pp. 1–21, 2022. DOI: 10.1002/mma.8178.
[26] A. Pantokratoras and E. Magyari, "EMHD free-convection boundary-layer flow from a Riga -plate," *J. Eng. Math.*, vol. 64, no. 3, pp. 303–315, 2009. DOI: 10.1007/s10665-008-9259-6.
[27] N. T. Eldabe, M. E. Gabr, A. Z. Zaher, and S. A. Zaher, "The effect of Joule heating and viscous dissipation on the boundary layer flow of a magnetohydrodynamics micropolar-nanofluid over a stretching vertical Riga plate," *Heat Trans.*, vol. 50, no. 5, pp. 4788–4805, 2020. DOI: 10.1002/htj.22102.
[28] A. Shafiq, F. Mebarek-Oudina, T. N. Sindhu and A. Abidi, "A study of dual stratification on stagnation point Walters' B nanofluid flow via radiative Riga plate: a statistical approach," *Eur. Phys. J. Plus*, vol. 136, no. 4, pp. 1–24, 2021. DOI: 10.1140/epjp/s13360-021-01394-z.
[29] T. Hayat, T. Abbas, M. Ayub, M. Farooq, and A. Alsaedi, "Flow of nanofluid due to convectively heated Riga plate with variable thickness," *J. Mol. Liq.*, vol. 222, pp. 854–862, 2016. DOI: 10.1016/j.molliq.2016.07.111.
[30] A. Naseem, A. Shafiq, L. Zhao, and M. U. Farooq, "Analytical investigation of third grade nanofluidic flow over a Riga plate using Cattaneo-Christov model," *Results Phys.*, vol. 9, pp. 961–969, 2018. DOI: 10.1016/j.rinp.2018.01.013.
[31] H. Vaidya, *et al.*, "Mixed convective nanofluid flow over a non-linearly stretched Riga plate," *Case Stud. Thermal Eng.*, vol. 24, pp. 100828, 2021. DOI: 10.1016/j.csite.2020.100828.
[32] E. E. Herrera-Valencia, *et al.*, "Study of the electroosmotic flow of a structured fluid with a new generalized rheological model," *Rheol. Acta*, vol. 63, pp. 3–32, 2023. DOI: 10.1063/1.5097867.
[33] L. A. Ramírez-Torres, E. E. Herrera-Valencia, M. L. Sánchez-Villavicencio, C. Soriano-Correa, V. J. Hernández-Abad, and F. Calderas, "Non-linear electro-rheological model of a membrane immersed in tanner-power law fluids applied to outer hair cells: shear-thinning mechanisms," *Phys. Fluids*, vol. 36, no. 3, pp. 033111 [1–16], 2024. DOI: 10.1063/5.0189731.
[34] A. Z. Zaher, K. K. Ali, and K. S. Mekheimer, "Electroosmosis forces EOF driven boundary layer flow for a non-Newtonian fluid with planktonic microorganism: Darcy Forchheimer model," *HFF*, vol. 31, no. 8, pp. 2534–2559, 2021. DOI: 10.1108/HFF-10-2020-0666.
[35] E. Magyari, M. E. Ali, and B. Keller, "Heat and mass transfer in the boundary layers on an exponentially stretching continuous surface," *J. Phys. D: Appl. Phys.*, vol. 38, no. 1-2, pp. 65–74, 1999. DOI: 10.1007/s002310000126.